Journal of Advanced Ceramics
2020, **9**(1): 83–93
https://doi.org/10.1007/s40145-019-0350-4
ISSN 2226-4108
CN 10-1154/TQ

Research Article

Highly conductive wear resistant Cu/Ti_3SiC_2(TiC/SiC) co-continuous composites via vacuum infiltration process

Dexuan YANG[a], Yu ZHOU[b], Xingheng YAN[a],
Honglei WANG[a], Xingui ZHOU[a,*]

[a] *Science and Technology on Advanced Ceramic Fibers and Composites Laboratory, National University of Defense Technology, Changsha 410073, China*
[b] *Department of Mechanical, Materials and Aerospace Engineering, Illinois Institute of Technology, Chicago 60616, USA*

Received: July 23, 2019; Revised: October 6, 2019; Accepted: October 6, 2019

Abstract: The MAX phase Ti_3SiC_2 has broad application prospects in the field of rail transit, nuclear protective materials and electrode materials due to its excellent electrical conductivity, self-lubricating properties and wear resistance. Cu–Ti_3SiC_2 co-continuous composites have superior performance due to the continuous distribution of 3D network structures. In this paper, the Cu/Ti_3SiC_2(TiC/SiC) co-continuous composites are formed via vacuum infiltration process from Cu and Ti_3SiC_2 porous ceramics. The co-continuous composites have significantly improved the flexural strength and conductivity of Ti_3SiC_2 due to the addition of Cu, with the conductivity up to 5.73×10^5 S/m, twice as high as the Ti_3SiC_2 porous ceramics and five times higher than graphite. The reaction between ingredients leads to an increase in the friction coefficient, while the hard reaction products (TiC_x, SiC) lower the overall wear rate (1×10^{-3} mm^3/(N·m)). Excellent electrical conductivity and wear resistance make co-continuous composites more advantageous in areas such as rail transit.

Keywords: Ti_3SiC_2; metal–ceramic co-continuous composites; vacuum infiltration; high conductive

1 Introduction

Ceramic/metal composites have excellent mechanical properties, electrical and thermal conductivity, as well as friction and wear properties. They can also be used as conductive, thermally conductive materials and wear-resistant materials in demanding environments. It is well known that ceramic matrix composites can further improve material properties. Brittle ceramic particle-strengthening and fiber-reinforcement have been utilized in an attempt to improve the strength and, particularly, the toughness [1]. The ceramic/metal composite materials reported at present are mainly ceramic particle reinforced metal matrix composite materials, and the preparation processes are mainly powder metallurgy, discharge plasma reaction sintering, and the like. Other than those reinforcement-matrix structures, co-continuous composites have a greater advantage, and this structural topology facilitates the design of the structure and properties of the material [2–5]. Both the reinforcement phase and the matrix have a continuous distribution of 3D network structures, which are independent and intersect each other,

* Corresponding author.
E-mail: 1455008455@qq.com

forming a network-like matrix and reinforcing phase interpenetrating composite material.

Co-continuous composite materials have received extensive attention. Caccia *et al.* [6] prepared ZrC/W co-continuous composite via reactive melt infiltration process, excellent thermal conductivity, high strength nickel-superalloy-based printed-circuit heat exchangers at a lower cost. Zhu *et al.* [7,8] prepared TiB_2–TiC/Cu–Ni anti-ablative materials by using titanium, boron carbide, copper powder, and nickel powder as raw materials from pressurization self-propagating high-temperature synthesis (SHS). Han *et al.* [9] synthesized ceramic/aluminum co-continuous ceramic and analyzed the effects of alloying additions and infiltration temperature. Chen and Breslin [10] prepared alumina/aluminum co-continuous composites with excellent wear resistant and high-temperature properties from a liquid-phase displacement reaction process. Daehn and Breslin [11] compared alumina/aluminum and alumina/aluminum–bronze co-continuous composites, and both materials showed good friction properties and thermal conductivity. Ramesh *et al.* [12] used reactive metal penetration method (RMP) to fabricate the SiC/Al co-continuous composites. Han and Feng [13] used spontaneous melt infiltration method to produce the SiC/Al co-continuous composites, and mixed a small amount of Mg into the Al alloy to reduce the infiltration temperature. Liu *et al.* [14] fabricated SiC/2024Al co-continuous composites having high flexural strength, fracture toughness, and hardness, with lamellar microstructure by freeze casting. Lei *et al.* [15] prepared TiC_x/Cu–Cu_4Ti co-continuous composites by infiltrating method, with compact structure and strong interface. The research of metal–ceramic co-continuous composite and different preparation processes provides design ideas for the preparation of composite materials.

Titanium silicon carbide (Ti_3SiC_2) is the MAX phase of ceramic. Different from traditional ceramic materials, Ti_3SiC_2 combines the merits of both metals and ceramics, such as machinability, good thermal and electrical conductivity, high strength, melting point, and thermal stability [16–19]. The ternary layered compounds have special physical and chemical properties, and their properties are unique from the abnormal valence bond structure. There are three valence bond structures in the crystal structure: covalent bond, ion bond, and metal bond. The general formula of ternary-layered MAX phase compounds is $M_{n+1}AX_n$ (M for transition metal elements, A for IIIA or IVA group elements, X for carbon or nitrogen elements, n = 1, 2, 3). According to n value, the compounds can be divided into three categories: n = 1, [211] phase, the general formula is M_2AX; n = 2, [312] phase, the general formula is M_3AX_2; n = 3, [413] phase, the general formula is M_4AX_3. The three types of MAX phase compounds have common structural characteristics, that is, the A layer atoms (composed of IIIA or IVA group elements) separate the $M_{n+1}X_n$ layer (composed of tightly stacked transition metal nitride or carbide). Therefore, it has similar plasticity, workability, heat conduction, electrical conductivity with metal materials, and similar physical and chemical properties with ceramic materials, such as high strength, high modulus, high melting point, oxidation resistance, corrosion resistance, high temperature resistance, and excellent thermal shock resistance [20,21]. Therefore, Ti_3SiC_2 has broad application prospects in the field of rail transit, nuclear protective materials, and electrode materials.

Turki *et al.* [22] used SiC/Ti powders as raw material to synthesize Ti_3SiC_2 by reactive spark plasma sintering (R-SPS) in the temperature range of 1300–1400 ℃. The increase of holding time was beneficial to the purity of Ti_3SiC_2, and the highest purity was 75%. The content of the second phase affected the microhardness and resistance of Ti_3SiC_2, and the higher the content was, the greater the microhardness was. Crisan and Crisan [23] deposited Cr–Al–C ternary MAX phase compound films on Si substrate by DC sputtering. The effects of substrate temperature and annealing in air on the crystallinity and oxidation of the films were investigated. Xu *et al.* [24] studied the tribological properties of *c*-axis textured shell-like Ti_3AlC_2 ceramics using a composite sliding ball with loads of 1, 5, and 9 N. It is found that the friction coefficient of the texture top surface corresponding to (000l) crystal plane is the lowest, while the friction rate of the texture measured surface is the lowest, 1.51×10^{-3} $mm^3/(N\cdot m)$, under 9 N load. The wear mechanisms are delamination, grain fracture, and grain spalling-off.

Ti_3SiC_2–Cu composites are mostly Ti_3SiC_2 particle-strengthening Cu matrix composites, and the preparation methods include powder metallurgy method [25–27] and spark plasma sintering (SPS) method [26–28]. In this paper, the Ti_3SiC_2–Cu co-continuous composites are fabricated from Ti_3SiC_2 porous ceramics and Cu by

vacuum infiltration process, showing higher flexural strength (270.21 MPa), better room-temperature electrical conductivity (5.73×10^5 S/m), and fracture toughness (5.9 MPa·$m^{1/2}$). The materials described herein are expected to be used to replace the materials used in high-speed railway pantograph. In general, the requirements of high-speed railway pantograph mainly reflect high electrical conductivity and high wear resistance. At present, graphite or copper-infiltrated graphite is mainly used for high-speed railway. The ceramic/metal composite in this paper is obviously higher in wear resistance, it also performs better in electrical conductivity prepared with the above two materials, and the preparation method of the metal/ceramic composite material based on titanium silicon carbide ceramic and copper is simple in process, stable in material properties, and convenient for large-scale production.

2 Experimental

2. 1 Preparation of specimens

The Ti_3SiC_2 porous ceramics start with mixing 85 wt% powders of Ti_3SiC_2 (particle size 200 mesh, 98%, Forsman Scientific (Beijing) Co., Ltd.) and 15 wt% powders of phenol-formaldehyde resin (PF, binder and pore former, particle size 80 mesh, Hunan Xiangbiao New Material Technology Co., Ltd.) in a planetary ball mill, rotating at the speed of 300 r/min for 3 h to get the mixed powders. The green bodies of porous ceramics are produced by temperature and pressure forming process in a stainless-steel mold on a curing press, under 10 MPa pressure for 30 min, where the powders of PF melt and wrap the powders of Ti_3SiC_2, then curing to shape the green bodies. The green bodies are heated at 650 ℃ for 1 h in nitrogen atmosphere to make PF carbonized to produce porous structure, and then sintered at 1440, 1460, 1480, 1500 ℃ for 2 h to get the porous ceramics. During the vacuum infiltration process, the degree of vacuum is above –100 kPa and temperature is 1400 ℃, lasting for 2 h, then the molten Cu can fully fill the open porosity of the porous ceramic to obtain co-continuous composites (Fig. 1).

2. 2 Characterization of specimens

The density and open porosity of porous ceramics and the density of co-continuous composites are measured by the Archimedes method with electronic balance (SE6001F) and kerosene (density is 0.8 g/cm^3 at 20 ℃, Tianjin Fuchen Chemical Reagents Factory). The theoretical density of co-continuous composites is calculated by Eq. (1). The room-temperature flexural strength and fracture toughness of specimens are tested by the three-point bending method (GBT 4741-1999 for flexural strength testing and GBT 23806-2009 for fracture toughness testing) with universal testing machine (WDW-100), the specimens are cut to be 3.0 mm × 4.0 mm × 40.0 mm for flexural strength testing and 3.0 mm × 6.0 mm × 40.0 mm with 3 mm incision for fracture toughness testing, and the test head speed is 0.5 mm/min for flexural strength testing and 0.05 mm/min for fracture toughness testing. The fracture surface morphology and microstructure of samples are characterized using a micro-computed tomography (Micro-CT, nanoVoxel-4000, the resolution is 0.5 μm), processed by AVISO software to reconstruct the 3D models, and a field-emission scanning electron microscopy (SEM, Hitachi SU8010). The phases of materials are analyzed by X-ray diffraction (XRD, D8 Advance) using a Cu Kα source, the scanning step size is 0.02° and the speed is 0.1 s/step. The conductivities of specimens are tested by four-point resistance tester (RTS-8). The friction and wear properties of co-continuous composites are tested using a multi-functional high-load material testing machine (MFT-5000, ball-disk friction pair) with loads of 20, 40, and 60 N. The Vickers hardness is measured by the micro-hardness tester (TI-950, Hysitron) under 5.0 mN load and the

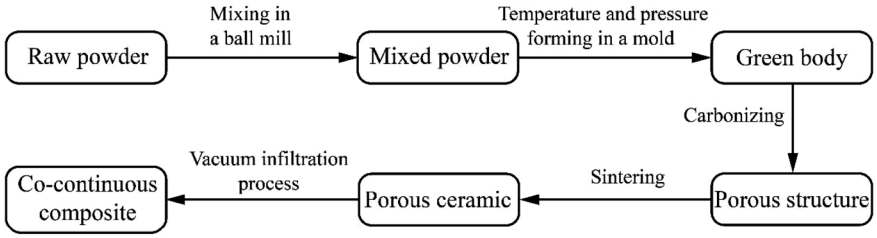

Fig. 1 Flow chart of the preparation of co-continuous composites.

loading rate is 10.0 mN/min, holding pressure for 10 s; the measurement results are averaged for three measurement points.

The equation of the theoretical density of the co-continuous composites is as following:

$$\rho_{cct} = \rho_{pc} + \rho_{Cu} \times \upsilon_{pc}/100 \quad (1)$$

The ρ_{cct} is the theoretical density of co-continuous composites, ρ_{pc} is the density of porous ceramics, ρ_{Cu} is the density of Cu (room temperature), and υ_{pc} is the porosity factor of porous ceramics.

3 Results and discussion

The properties and structure of the Ti_3SiC_2 porous ceramic have an effect on the structure and properties of the metal–ceramic co-continuous composite. The open porosity and pore structure of the Ti_3SiC_2 porous ceramics determine the content and structure of metal phase in meta–ceramic co-continuous composite, which affects the properties of the composite. Therefore, this paper characterizes and analyzes the properties of Ti_3SiC_2 porous ceramics and the properties of metal–ceramic co-continuous composites.

3.1 Characterization of Ti_3SiC_2 porous ceramics

The microstructures of porous ceramics are shown in Fig. 2. The three-dimensional topology of these interconnected open porous determines the structure of the Cu phase in the co-continuous composites and also provides the possibility for molten Cu to fully penetrate into the porous ceramic. However, the appearance of

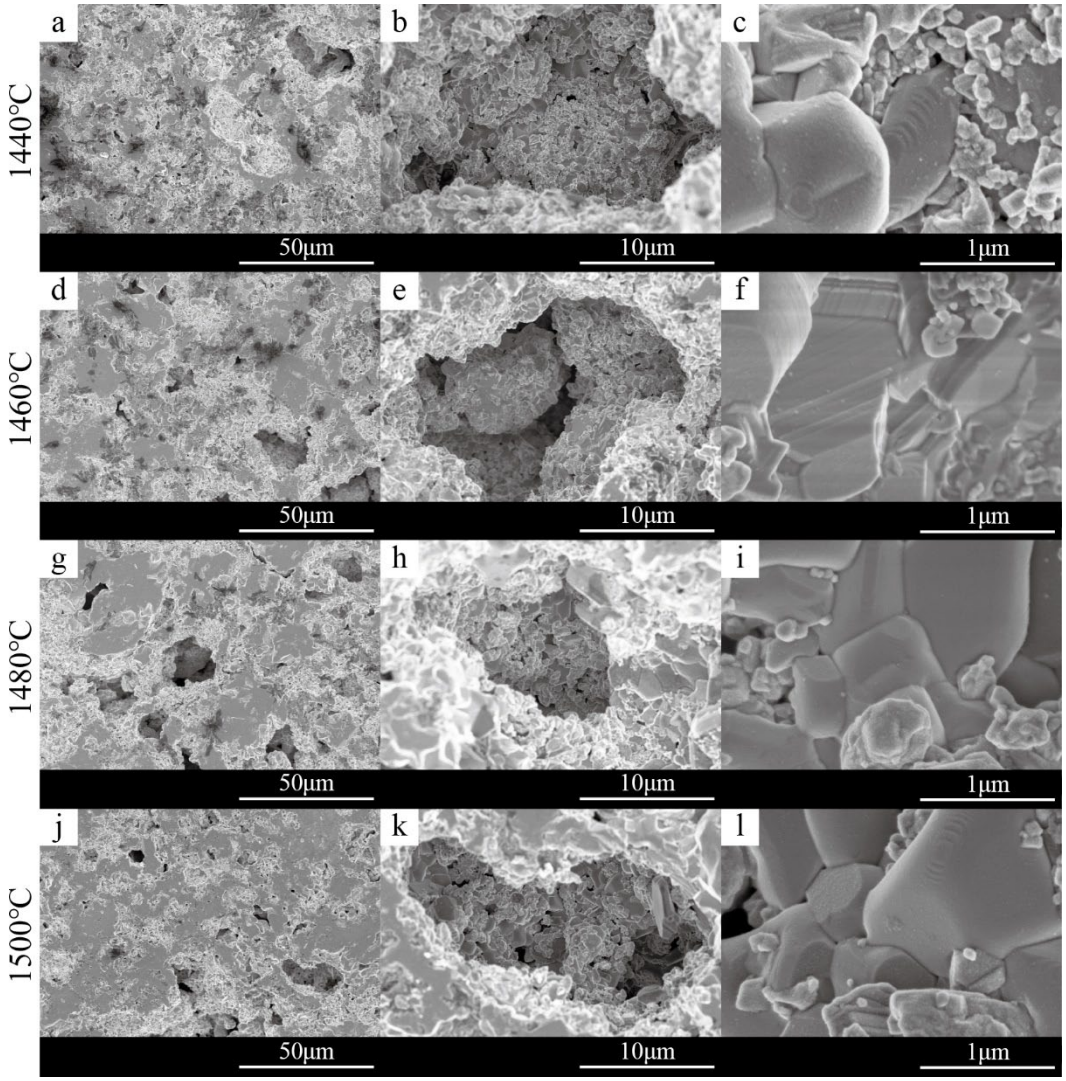

Fig. 2 Microstructure of porous ceramics sintered at 1440, 1460, 1480, 1500 ℃: (a, d, g, j) the overall appearance of the pores, (b, e, h, k) open pores, and (c, f, i, l) Ti_3SiC_2 particles.

closed pores causes stress concentration and reduces the mechanical properties of the co-continuous composites. The layered structure of the MAX phase Ti_3SiC_2 can be clearly seen on the microscopic morphology of the ceramic particles (Figs. 2(c), 2(f), 2(i), and 2(l)). The surface of the particles has patterns like terraced fields, different particles with different directions and angles. The atoms of particles diffuse between each other during the sintering process, and the adhesion between particles can also be seen.

The density and open porosity of Ti_3SiC_2 porous ceramics (Table 1) show no connection with sintering temperature. The open pores of the porous ceramics are mainly produced by the carbonization of the PF (Figs. 2(b), 2(e), 2(h), and 2(k)) and the gaps between Ti_3SiC_2 particles produce partially closed pores. The particle size and mass fraction of the PF powders affect the pore size and porosity of the porous ceramic, which in turn affect the composite structure. The porosity of pores formed by 200 mesh Ti_3SiC_2 particles stacking and 15 wt% 80 mesh PF powder carbonization is about 35.14%±0.26%. Physical characteristics such as pore size and porosity can be designed by changing the size of ceramic particles and the content of phenolic resin. With the increase of PF powder content, the ceramic porosity and the metal phase content increase, the structure, properties, and performance of the composite material change, so that the topology of the co-continuous composites can be designed by a simple way to achieve the design of the properties. How these variables affect the pores is not discussed in this paper and is worth further research.

The XRD pattern (Fig. 3) shows that, during carbonization and sintering process, the powders of Ti_3SiC_2 reacted with the carbons which carbonized from the powders of PF in the green bodies into TiC_x (49.7±2.3 wt%) and SiC (25.7±2.8 wt%) with 24.7±0.9 wt% Ti_3SiC_2 left (reaction (2)) because the increase of C content leads to a change in the equilibrium point of the Ti–Si–C ternary phase diagram [29,30]. In this process, the carbons are completely reacted with Si

Table 1 Density and open porosity of porous ceramics

Temperature of sintering, T_s (℃)	Density, ρ_{pc} (g·cm^{-3})	Open porosity, υ_{pc} (%)
1440	2.82	34.88
1460	2.82	35.04
1480	2.84	35.34
1500	2.84	35.29

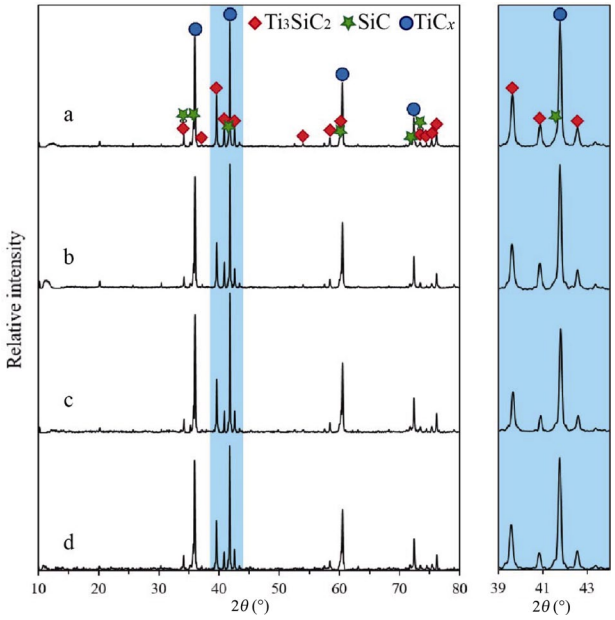

Fig. 3 XRD patterns of porous ceramics at different sintering temperature: (a) 1440 ℃, (b) 1460 ℃, (c) 1480 ℃, (d) 1500 ℃.

layer (the A of the MAX phase) in the Ti_3SiC_2, so that the contents of TiC_x and SiC are consistent at different sintering temperature.

$$Ti_3SiC_2 + C \rightarrow TiC_x + SiC \quad (2)$$

The Ti_3SiC_2 porous ceramic exhibits a brittle fracture form in the three-point flexural strength test at room temperature (RT), as shown by the load–displacement curve of the porous ceramic sintering at 1480 ℃ (Fig. 4(a)), and the flexural strength is the highest at this temperature, 91.27±2.73 MPa (Fig. 4(b)). It can be seen from the trend of the flexural strength as a function of the sintering temperature that the flexural strength has a maximum value. When the sintering temperature is lower than 1480 ℃, the flexural strength increases with the increase of temperature, but when the sintering temperature is higher than 1480 ℃, the flexural strength decreases with the increase of temperature.

The micro-morphology of the porous ceramic fracture surface is shown in Fig. 5. The fracture site of the porous ceramic is mainly the part of the powder particles that are connected to each other when sintering, and the fracture form is intergranular fracture, because the cross-sectional area of the joint is small, stress concentration occurs, and the bonding force of the part is smaller than that of the interior of the particle.

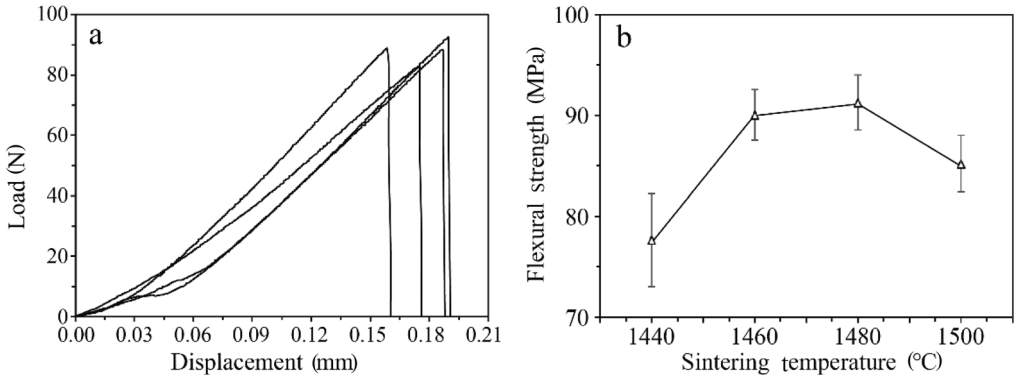

Fig. 4 Flexural strength of porous ceramics at RT: (a) load–displacement curves of samples sintering at 1480 ℃, (b) flexural strength.

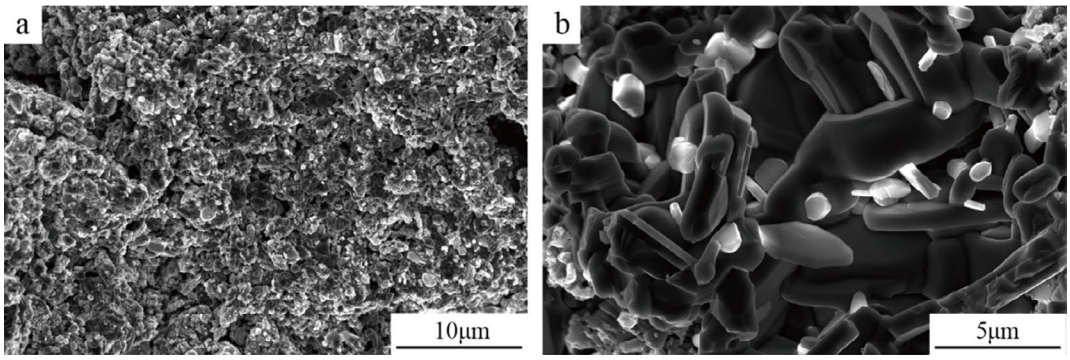

Fig. 5 Fracture surface morphology of the porous ceramic (the samples in the figure are sintering at 1480 ℃).

3. 2 Characterization of metal–ceramic co-continuous composites

The Cu melts at 1083 ℃ and exhibits excellent wettability to Ti_3SiC_2 when the temperature is above 1270 ℃ and the contact angle is 15.1°. The molten Cu reacts with Ti_3SiC_2 to form TiC_x and Cu_xSi_y (reaction (3)) [31]. The wetting between liquid metal and ceramic is mainly achieved by interfacial reaction to form interfacial reaction products. Therefore, the molten Cu can fully wet porous Ti_3SiC_2 ceramics and fill pores at 1400 ℃, –100 kPa. Excellent wettability of copper to Ti_3SiC_2 ceramic is a favorable condition for preparing metal–ceramic co-continuous composites via vacuum infiltration process.

$$Ti_3SiC_2 + Cu \rightarrow TiC_x + Cu_xSi_y \quad (3)$$

The Micro-CT 3D models of co-continuous composites are shown in Fig. 6(a) and the microstructure of cross-section of the co-continuous composites is shown in Figs. 6(b) and 6(c). The cross-sectional gray-scale images of Micro-CT are processed by AVISO software to reconstruct 3D models. They are segmented into two parts according to the gray-scale value of the scanned image. The lower density parts have lower gray value and darker color in the CT images, corresponding to ceramic phases, on the contrary corresponding to metal phases. The analysis of the Micro-CT model of continuous composites shows that the volume fraction of copper and ceramics is 34.6 and 65.4 vol%, respectively, consistent with the porous ceramic porosity test results by the Archimedes method. The Cu and ceramics are uniformly distributed on the cross-section of the co-continuous composites, and Cu has sufficiently filled the open pores of the porous ceramics. Excellent wettability and interfacial reaction between two phases allow the two phases to be firmly bonded together.

The porous ceramic exhibits a brittle fracture form in the three-point flexural strength test, as shown by the load–displacement curve of the porous ceramic sintering at 1480 ℃.

The load–displacement curve and flexural strength of the co-continuous composite material at room temperature are shown in Fig. 7. Due to the addition of the copper phase, the load–displacement curve of the composite exhibits a certain degree of toughness, and the flexural strength is greatly improved compared

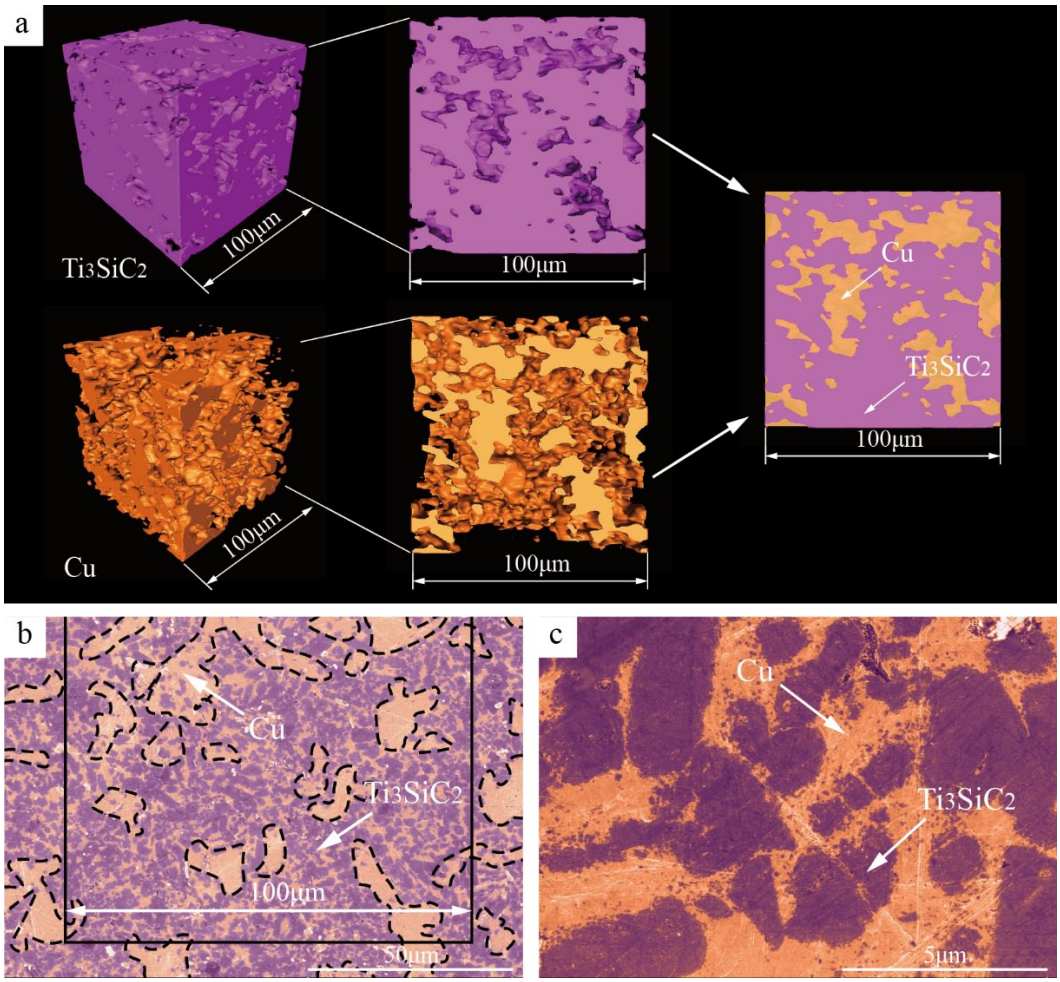

Fig. 6 Microstructure of metal–ceramic co-continuous composites (the samples in the figure are sintering at 1480 ℃): (a) Micro-CT model of co-continuous composites, (b, c) SEM images of cross-section of co-continuous composites surface.

Table 2 Density and theoretical density of co-continuous composites

Temperature of sintering, T_s (℃)	Density, ρ_{cc} (g·cm^{-3})	Theoretical density, ρ_{cct} (g·cm^{-3})
1440	5.41	5.98
1460	5.65	5.99
1480	5.72	5.97
1500	5.85	5.98

with the porous ceramic; the most upper flexural strength is 270.21±5.30 MPa with fracture toughness of 5.9 MPa·m$^{1/2}$ (Fig. 8). The flexural strength varies with the sintering temperature and is similar to that of porous ceramics. It can be seen that the mechanical properties of the co-continuous composites have a great correlation with the porous ceramics.

Figure 9 shows a typical load–displacement curve in the fracture toughness test of composites (sintering at 1480 ℃); as the displacement increases, the load of the co-continuous composites first reaches a peak, and then rapidly drops to an inflection point. After the inflection point, the load slowly decreases as the displacement increases. This non-brittle fracture mode indicates the toughening mechanism of the co-continuous composites during the fracture process.

The fracture surface morphology of the co-continuous composites is taken as shown in Fig. 10. When the metal phase breaks, large plastic deformation occurs. The addition of the metal phase into porous ceramic increases the flexural strength, and a large amount of energy can be absorbed during the plastic deformation process. When metal copper fills the porous ceramic pores, the gaps among ceramic particle filled metal, which can effectively reduce stress concentration, prevent the crack from expanding in the ceramic phase, and improve the toughness of the composite. The ceramic phase fracture form is cleavage fracture, and the crack propagates along the interlayer of the MAX

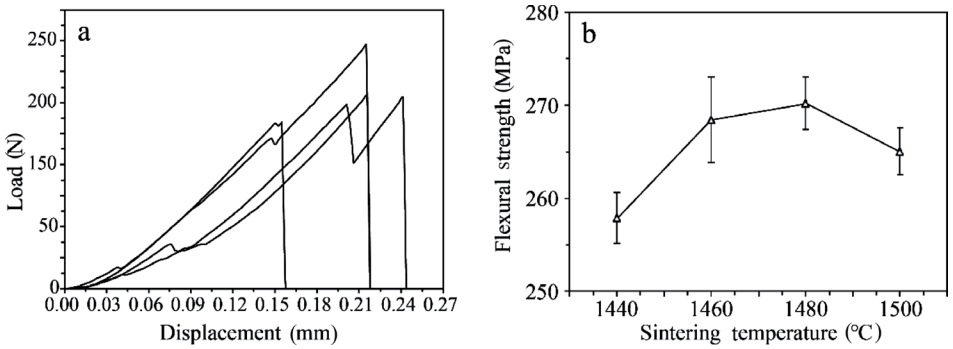

Fig. 7 Flexural strength of co-continuous composites at RT: (a) load–displacement curves, (b) flexural strength.

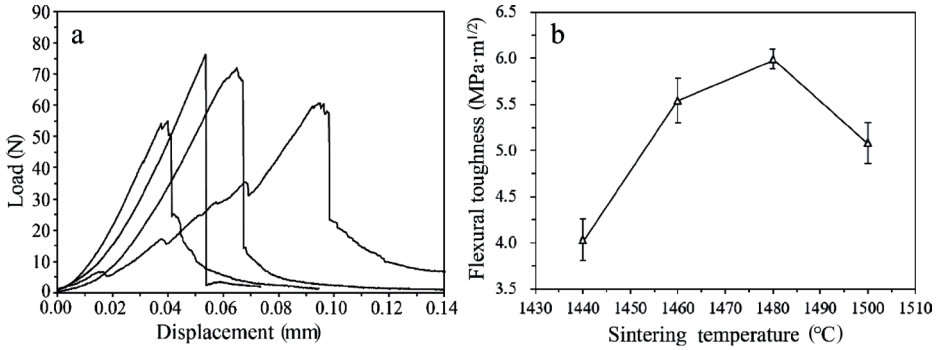

Fig. 8 Flexural toughness of co-continuous composites: (a) load–displacement curves, (b) flexural toughness.

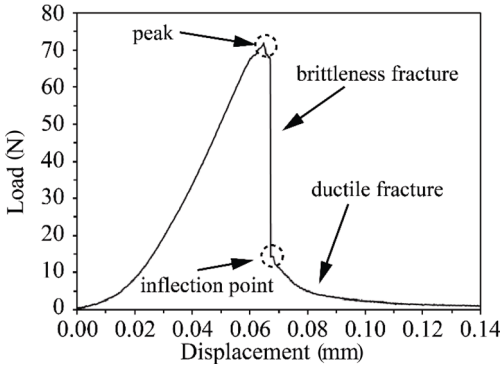

Fig. 9 A typical load–displacement curve of co-continuous composites (sintering at 1480 ℃) in fracture toughness test.

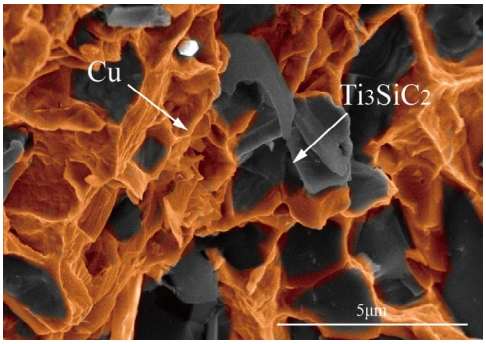

Fig. 10 Fracture surface morphology of the co-continuous composites.

phase layer structure. This structure makes the section have distinct layered cleavage steps. The ceramic phase has a high modulus and therefore withstands greater stress and breaks first when subjected to external forces.

In conclusion, according to the mechanical properties of the samples, the optimum sintering temperature of the green bodies can be obtained at 1460–1480 ℃.

3.3 Conductivity of porous ceramics and co-continuous composites

Ti_3SiC_2 has good electrical properties (3.7×10^6 S/m) due to its layered structure, which is similar to graphite and the delocalized electrons, which is parallel to the plane of the silicon layer, and Cu is also a good conductor of electricity. Therefore, the composites combined with them are likely to have better electrical properties. We measured the electrical conductivity of porous ceramics (Table 3) at room temperature, and samples are cut to 25 mm in diameter and 5 mm in thickness. The results show that as the sintering temperature increases, the electrical properties of the sample increase. When the sintering temperature is higher than 1460 ℃, the electrical conductivity reaches and stabilizes at 2.63×10^5 S/m. The same is shown with

Table 3 Conductivity of porous ceramics and co-continuous composites

Porous ceramics		Co-continuous composites
Temperature of sintering, T_s (℃)	Conductivity ($S \cdot m^{-1}$)	Conductivity ($S \cdot m^{-1}$)
1440	2.08×10^5	5.40×10^5
1460	2.56×10^5	5.55×10^5
1480	2.63×10^5	5.72×10^5
1500	2.63×10^5	5.73×10^5

the co-continuous composites, conductivity increases before 1460 ℃ and peaks at 5.73×10^5 S/m, twice as high as the porous ceramics and five times higher than graphite ($(0.7–1.2)\times10^5$ S/m, room temperature). The excellent electrical properties give the Ti_3SiC_2/Cu co-continuous composites prepared in this paper application prospects in the fields of rail transit and electrode materials, etc.

3. 4 Friction and wear properties of co-continuous composites

The friction and wear properties of materials are often related to the hardness of the material. The Vickers microhardness measured for the ceramic phase and the metal phase is shown in Table 4. The Vickers hardness of the ceramic phase is at least 25.6±0.33 GPa, which is equivalent to the hardness of TiC (about 27 GPa) and SiC (about 22.2 GPa). The higher hardness is due to the enhancement of high hardness TiC and SiC. The Vickers hardness measured by monolithic Ti_3SiC_2 in the reference is about 5.02 GPa. The Vickers hardness of the ceramic phase has certain regularity with the sintering temperature of the porous ceramic. With the increase of temperature, the Vickers hardness decreases first and then increases, which is negatively correlated with the variation of the flexural strength of the porous ceramic. Although high hardness means higher strength,

Table 4 Vickers hardness of different phases

Temperature of sintering (℃)	Vickers hardness (GPa)	
	Cu phase	Ti_3SiC_2 phase
1440	3.79±0.22	29.31±0.33
1460	3.81±0.19	25.65±0.34
1480	3.74±0.37	25.78±0.10
1500	3.35±0.19	29.96±0.46

it also increases the brittleness of the material, resulting in a lower flexural strength of the material than the hardness. The Vickers hardness of the metal phase is about 3.7±0.32 GPa, which has no obvious correlation with the change of sintering temperature, and the metal phase with low hardness plays a toughening effect in the composite material.

The friction and wear properties of co-continuous composites are tested using ball–disk friction pair, and the friction coefficient–pressure curve is shown in Fig. 12. The samples (25 mm in diameter and 5 mm in thickness) are tested under a load of 20, 40, 60 N, and it can be seen that as the load increases, the friction coefficient of the samples shows a downward trend, and the average friction coefficient decreases from 0.97 to 0.69. Under the load of ball–disk friction pair, the shearing force causes the surface material of the samples to be destroyed, the resistance becomes larger, and then the average friction coefficient is higher. As the load increases, the average friction coefficient decreases. It is possible that the layered-structure ceramic phases form fragments under the action of shear force, and this kind of debris lubricates the friction pair, thereby reducing the sliding friction force and thus reducing the friction coefficient. Through the comparison with the friction coefficients of different sintering temperature samples, it can be seen that under the same load, the friction coefficient of the sample

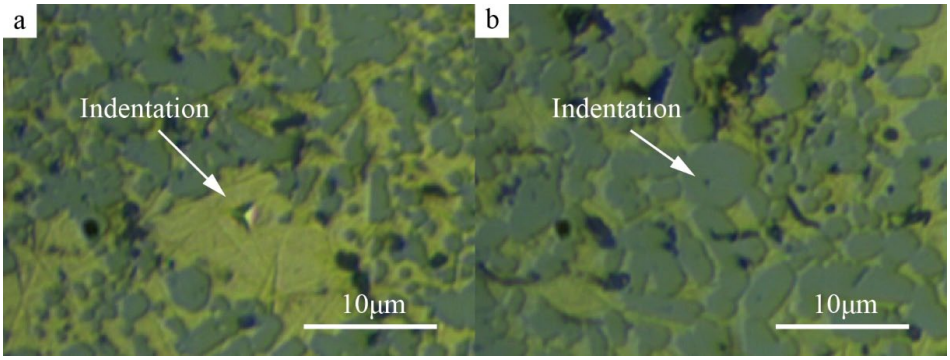

Fig. 11 Micrograph of micro-hardness test: (a) indentation on the metal phase, (b) indentation on the ceramic phase.

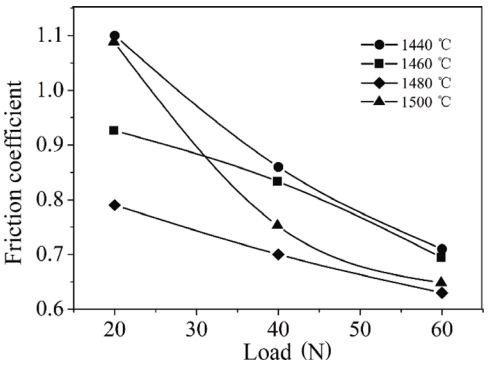

Fig. 12 Friction coefficient–pressure curve of the co-continuous composites.

Table 5 Wear rate of co-continuous composites

Temperature of sintering (℃)	Wear rate ($mm^3/(N·m)$)
1440	0.63×10^{-3}
1460	3.30×10^{-3}
1480	1.10×10^{-3}
1500	1.65×10^{-3}

with sintering temperature of 1480 ℃ is lower, and the lowest friction coefficient is 0.63 under 60 N; the friction coefficient of the sample with the sintering temperature of 1440 ℃ is the highest, and when the load is 20 N, the friction coefficient is even more than 1, which is 1.10. Through the comparison with Vickers hardness test results, it can be seen that the sample with high hardness has a large friction coefficient. The lubricity of co-continuous composites is poor, and sharp noise can be heard during the friction test. It is speculated that TiC and SiC exist in the ceramics and Cu reacts with Ti_3SiC_2 to form hard phases during the vacuum infiltration process [28]. These hard phases cause the friction surface to fail to form a self-lubricating film with a high coefficient of friction [27]. It is also that these hard phases make the composites more resistant to wear; the wear rate is only 1.67×10^{-3} $mm^3/(N·m)$ in average (Table 5).

4 Conclusions

(1) The optimum sintering temperature of porous ceramics Ti_3SiC_2 is 1480 ℃; at this sintering temperature, the porous ceramics have the highest strength (91.27± 2.73 MPa) and the highest conductivity (2.63×10^5 S/m).

(2) Porous ceramics can be prepared by using a suitable resin, which can be pressed and formed at a temperature of less than 300 ℃ and the process is stable and reliable. The resin has two functions, as a molding adhesive, to ensure good formability of the green body; it can also be converted into carbon by pyrolysis, and act as a carbon source to function as a pore-forming agent and adjust the reactivity in the green body. This research creatively imparts new functions to conventional adhesives.

(3) The Cu/Ti_3SiC_2(TiC/SiC) co-continuous composites via vacuum infiltration process have good performance. The Cu/Ti_3SiC_2(TiC/SiC) co-continuous composites have significantly improved flexural strength and conductivity due to the addition of Cu, a flexural strength of 270.21±5.30 MPa, fracture toughness of 5.9 $MPa·m^{1/2}$, and conductivity of 5.73×10^5 S/m, five times higher than graphite.

(4) The reaction between carbon and Ti_3SiC_2 and the reaction between Cu and Ti_3SiC_2 produce hard phases that result in a high coefficient of friction (0.7) but low wear rate (1.67×10^3 $mm^3/(N·m)$).

(5) The metal phase and the ceramic phase are continuous in the composite material, which can maintain the advantages of both metal and ceramic. On one hand, it has the toughness and high electrical conductivity and high thermal conductivity of the metal; on the other hand, it maintains the high wear resistance and low expansion of the ceramic. Excellent wear resistance, electrical properties, and mechanical properties give Cu/Ti_3SiC_2(TiC/SiC) co-continuous composite materials broad application prospects in the field of rail transit, nuclear field, and battery electrode materials. The shortcoming of the composites, high friction coefficient, requires further research.

References

[1] Donald IW, McMillan PW. Ceramic-matrix composites. *J Mater Sci* 1976, **11**: 949–972.

[2] Wang LF, Lau J, Thomas EL, *et al*. Co-continuous composite materials for stiffness, strength, and energy dissipation. *Adv Mater* 2011, **23**: 1524–1529.

[3] Chang H, Binner J, Higginson R, *et al*. High strain rate characteristics of 3-3 metal–ceramic interpenetrating composites. *Mat Sci Eng A* 2011, **528**: 2239–2245.

[4] Yin LY, Zhou XG, Yu JS, *et al*. Fabrication of a polymer composite with high thermal conductivity based on sintered silicon nitride foam. *Compos Part A: Appl Sci Manuf* 2016, **90**: 626–632.

[5] Mazerolles T, Heuzey MC, Soliman M, *et al*. Development of co-continuous morphology in blends of thermoplastic starch and low-density polyethylene. *Carbohydr Polym* 2019, **206**: 757–766.

[6] Caccia M, Tabandeh-Khorshid M, Itskos G, *et al*. Ceramic–metal composites for heat exchangers in concentrated solar power plants. *Nature* 2018, **562**: 406–409.
[7] Zhu CC, He XD, Qu W. Properties of TiC–TiB_2/Cu–Ni composites prepared by SHS. *J Harbin Inst Tech* 2003, **35**: 953–957. (in Chinese)
[8] Zhu CC, Li Y, He XD, *et al*. Study on the behavior in thermal shock and ablation resistance of TiC–TiB_2/Cu ceramic-matrix composite. *J Aeronaut Mater* 2003, **23**: 15–19. (in Chinese)
[9] Han GW, Feng D, Yin M, *et al*. Ceramic/aluminum co-continuous composite synthesized by reaction accelerated melt infiltration. *Mat Sci Eng A* 1997, **225**: 204–207.
[10] Chen MY, Breslin MC. Friction behavior of co-continuous alumina/aluminum composites with and without SiC reinforcement. *Wear* 2001, **249**: 868–876.
[11] Daehn GS, Breslin MC. Co-continuous composite materials for friction and braking applications. *JOM* 2006, **58**: 87–91.
[12] Ramesh R, Prasanth AS, Ragavan M, *et al*. SiC/aluminium co-continuous composite synthesized by reactive metal penetration. *Appl Mech Mater* 2014, **592–594**: 847–853.
[13] Han G, Feng D. Synthesis of SiC/Al co-continuous composite by spontaneous melt infiltration. *J Mater Sci Technol* 2000, **16**: 466–470.
[14] Liu Q, Ye F, Gao Y, *et al*. Fabrication of a new SiC/2024Al co-continuous composite with lamellar microstructure and high mechanical properties. *J Alloys Compd* 2014, **585**: 146–153.
[15] Lei C, Zhai HX, Huang ZY, *et al*. Fabrication, microstructure and mechanical properties of co-continuous TiC_x/Cu–Cu_4Ti composites prepared by pressureless-infiltration method. *Ceram Int* 2019, **45**: 2932–2939.
[16] Sun ZM, Yi Z, Zhou YC. Synthesis of Ti_3SiC_2 powders by a solid–liquid reaction process. *Scripta Mater* 1999, **41**: 61–66.
[17] Zhou YC, Sun ZM. Temperature fluctuation/hot pressing synthesis of Ti_3SiC_2. *J Mater Sci* 2000, **35**: 4343–4346.
[18] Sun ZM, Zhou YC. Tribological behavior of Ti_3SiC_2-based material. *J Mater Sci Technol* 2002, **18**:142–145.
[19] Zhang HB, Bao YW, Zhou YC. Current status in layered ternary carbide Ti_3SiC_2, a review. *J Mater Sci Technol* 2009, **25**: 1–38.
[20] Liu JJ, Li SL. New research progress of layered ceramic Ti_3SiC_2. *Mat Sci Eng Powder Metal* 2006, **11**: 63–69.
[21] Wang XH, Zhou YC. Layered machinable and electrically conductive Ti_2AlC and Ti_3AlC_2 ceramics: A review. *J Mater Sci Technol* 2010, **26**: 385–416.
[22] Turki F, Abderrazak H, Schoenstein F, *et al*. Physico-chemical and mechanical properties of Ti_3SiC_2-based materials elaborated from SiC/Ti by reactive spark plasma sintering. *J Adv Ceram* 2019, **8**: 47–61.
[23] Crisan O, Crisan AD. Incipient low-temperature formation of MAX phase in Cr–Al–C films. *J Adv Ceram* 2018, **7**: 143–151.
[24] Xu LD, Zhu DG, Grasso S, *et al*. Effect of texture microstructure on tribological properties of tailored Ti_3AlC_2 ceramic. *J Adv Ceram* 2017, **6**: 120–128.
[25] Xie H, Ngai TL, Zhang P, *et al*. Erosion of Cu–Ti_3SiC_2 composite under vacuum arc. *Vacuum* 2015, **114**: 26–32.
[26] Zhang P, Ngai TL, Wang AD, *et al*. Arc erosion behavior of Cu–Ti_3SiC_2 cathode and anode. *Vacuum* 2017, **141**: 235–242.
[27] Dang WT, Ren SF, Zhou JS, *et al*. The tribological properties of Ti_3SiC_2/Cu/Al/SiC composite at elevated temperatures. *Tribol Int* 2016, **104**: 294–302.
[28] Dang WT, Ren SF, Zhou JS, *et al*. Influence of Cu on the mechanical and tribological properties of Ti_3SiC_2. *Ceram Int* 2016, **42**: 9972–9980.
[29] Arunajatesan S, Carim AH. Synthesis of titanium silicon carbide. *J Am Ceram Soc* 1995, **78**: 667–672.
[30] Radhakrishnan R, Williams J, Akinc M. Synthesis and high-temperature stability of Ti_3SiC_2. *J Alloys Compd* 1999, **285**: 85–88.
[31] Lu JR, Zhou Y, Li HY, *et al*. Wettability and wetting process in Cu/Ti_3SiC_2 system. *J Inorg Mater* 2014, **29**: 1313–1319.